Astron. Astrophys. 357, 931–937 (2000)

ASTRONOMY AND ASTROPHYSICS

Lithium and rotation on the subgiant branch

II. Theoretical analysis of observations

J.D. do Nascimento Jr.[1,4], **C. Charbonnel**[1], **A. Lèbre**[2], **P. de Laverny**[3], **and J.R. De Medeiros**[4]

[1] Laboratoire d'Astrophysique de Toulouse, UMR 5572 CNRS, 16 Avenue E. Belin, 31400 Toulouse, France
[2] GRAAL, UPRES–A 5024 CNRS, CC 072, Université Montpellier II, 34095 Montpellier Cedex, France
[3] Observatoire de la Côte d'Azur, Fresnel, UMR6528, B.P. 4229, 06304 Nice CEDEX 4, France
[4] Departamento de Física, Universidade Federal do Rio Grande do Norte, 59072-970 Natal, R.N., Brazil

Received 2 June 1999 / Accepted 25 February 2000

Abstract. Lithium abundances and rotation, determined for 120 subgiant stars in Lèbre et al. (1999) are analyzed. To this purpose, the evolutionary status of the sample as well as the individual masses have been determined using the HIPPARCOS trigonometric parallax measurements to locate very precisely our sample stars in the HR diagram. We look at the distributions of $A_{\rm Li}$ and *Vsini* with mass when stars evolve from the main sequence to the subgiant branch.

For most of the stars in our sample we find good agreement with the dilution predictions. However, the more massive cool stars with upper limits of Li abundances show a significant discrepancy with the theoretical predictions, even if the Non-LTE effects are taken into account. For the rotation behaviour, our analysis confirms that low mass stars leave the main sequence with a low rotational rate, while more massive stars are slowed down only when reaching the subgiant branch. We also checked the connection between the observed rotation behaviour and the magnetic braking due to the deepening of the convective envelope. Our results shed new light on the lithium and rotation discontinuities in the evolved phase.

Key words: convection – stars: abundances – stars: evolution – stars: interiors – stars: late-type – stars: rotation

1. Introduction

This paper is the second in a series about the study of lithium and rotation in evolved stars based on both new high resolution spectroscopic observations and precise rotational velocities obtained with the CORAVEL spectrometer. In Lèbre et al. (1999, hereafter Paper I) we derived lithium abundances by spectral synthesis analysis and presented the observational data for a large and homogeneous sample of F, G, and K-type Population I subgiant stars. On the basis of this uniform data set, we could confirm the occurrence of the rotational discontinuity near the spectral type F8IV (Gray & Nagar 1985; De Medeiros & Mayor 1989, De Medeiros 1990), and localize a lithium drop-off around the spectral type G2IV. No clear correlation appeared between the lithium abundance and the rotational velocity (see also De Medeiros et al. 1997).

In the present work we investigate the physical processes that underline the lithium and rotational discontinuities along the subgiant branch. For this purpose we first determine the evolutionary status and individual masses of our sample stars by using the HIPPARCOS parallaxes and by comparing the observational Hertzsprung-Russell diagram with evolutionary tracks computed with the Toulouse-Geneva code (Sect. 2). This allows us to study very precisely the behaviour of the lithium abundance and of the rotational velocity as a function of effective temperature, stellar mass, metallicity and evolutionary stage. The lithium main features are discussed in Sect. 3 where we compare the observations with theoretical predictions related to the dilution mechanism (Iben 1967a,b). Finally, the connection between the observed rotation behaviour and the magnetic braking due to the deepening of the convective envelope (Gray 1981; Gray & Nagar 1985) is quantified in Sect. 4. This study, based on a close examination of the stellar parameters, sheds new light on the question of the link between rotation and lithium discontinuities in subgiant stars.

2. Observational data and evolutionary status

2.1. Working sample

Our analysis is based on the observational data from Paper I. This sample is composed of 120 Pop I subgiant stars with F, G and K spectral types which belong to the "Catalogue of rotational and radial velocities for evolved stars" (De Medeiros & Mayor 1999), as well as to the Bright Star Catalogue (Hoffleit & Jaschek 1982). We thus use the rotational velocities given in Paper I, as well as the values derived for $\log g$, $A_{\rm Li}$ and $T_{\rm eff}$ with their respective errors.

2.2. Evolutionary status

In order to interpret the observations accurately, we need to know the mass and the evolutionary stage of the sample stars.

Send offprint requests to: J.D. do Nascimento Jr. (dias@obs-mip.fr)

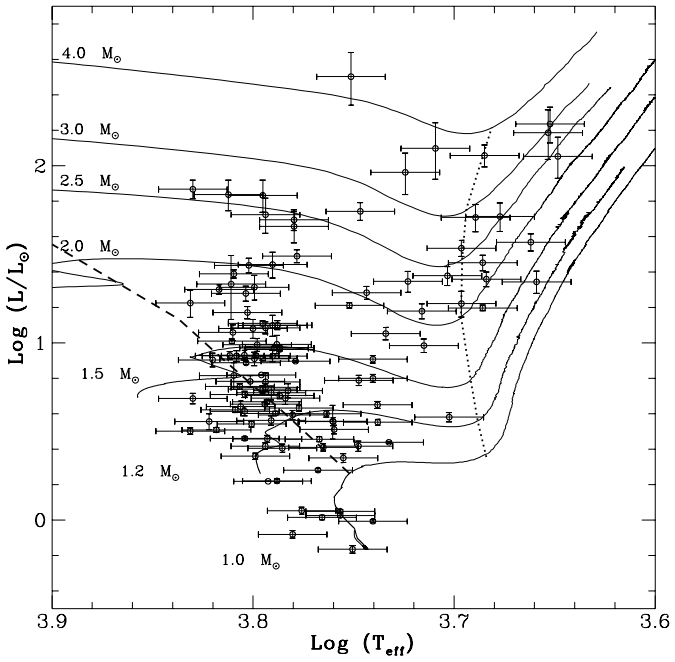

Fig. 1. Distribution of the sample stars in the HR diagram. Luminosities and related errors have been derived from the Hipparcos parallaxes. The typical error on $T_{\rm eff}$ is $\pm$ 200 K (Paper I). Evolutionary tracks at [Fe/H]=0 are shown for stellar masses between 1 and 4 $M_{\odot}$. The turnoff and the beginning of the ascent on the red giant branch are indicated by the dashed and dotted lines respectively in order to discriminate dwarfs, subgiants and giants

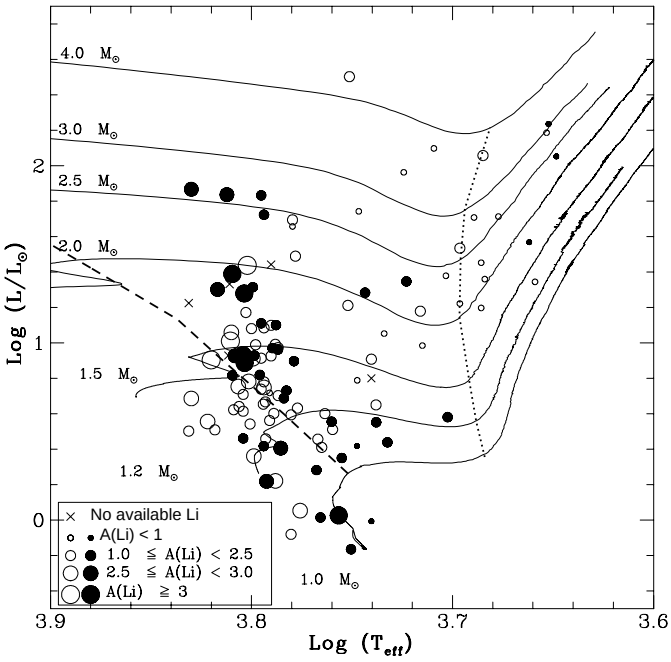

Fig. 2. Distribution of the Li abundances in the HRD. Single and binary stars are identified with open and filled circles respectively. The size of the circles is proportional to the Li abundances quoted in Paper I. Crosses refer to stars without any available Li abundance. Evolutionary tracks, as well as the dashed and dotted lines are as in Fig. 1

We use the HIPPARCOS (ESA 1997) trigonometric parallax measurements to locate precisely our objects in the HR diagram. Among our 120 stars, only one object (HD 144071) has no available Hipparcos parallax and is thus rejected from further analysis. Intrinsic absolute magnitudes $M_{\rm V}$ are derived from the parallaxes and the $m_{\rm V}$ magnitudes given by Hipparcos. We determine the bolometric corrections BC by using the Buser & Kurucz's relation (1992) between BC and V-I (again taken from the Hipparcos Catalogue). Finally, we compute the stellar luminosity and the associated error from the sigma error on the parallax. The uncertainties in luminosity lower than ± 0.1 have an influence of ± 0.4 in the determination of the masses. We show the results of these determinations in Fig. 1 and in Table 1. This table displays the stellar masses and luminosities derived for all objects of our sample. Moreover complementary data used for the present analysis (*Vsini*, $T_{\rm eff}$, log g , [Fe/H] and $A_{\rm Li}$) can be found in Papier I (see Tables 1 to 3). The error adopted on $T_{\rm eff}$ ($\pm$200K) is typical for this class of stars, as already discussed in Paper I.

We have computed evolutionary tracks with the Toulouse-Geneva code for a range of stellar masses between 1 and 4 $M_{\odot}$ and for different metallicities consistent with the range of our sample stars (see Paper I). However, solar composition being relevant to most of the objects of our sample (about 65%), only tracks computed with [Fe/H]=0 will be displayed in the figures. The evolution was followed from the Hayashi fully convective configuration. We used the radiative opacities by Iglesias & Rogers (1996), completed with the atomic and molecular opacities by Alexander & Ferguson (1994). The nuclear reactions are from Caughlan & Fowler (1988) and the screening factors are included according to the prescription by Graboske et al. (1973). No transport processes except for the classical convective mixing (with a value of 1.6 for the mixing length parameter) are taken into account.

2.3. Discrimination between dwarfs, subgiants and giants among the sample

In Fig. 1 we compare the observational HR diagram with the evolutionary tracks computed with [Fe/H] = 0. The dashed line indicates the evolutionary point where the subgiant branch starts and which corresponds to the hydrogen exhaustion in the stellar central regions (i.e., turnoff point). About 30 stars are located below the turnoff line and therefore appear to be genuine dwarfs, although classified as subgiants in the Bright Star Catalogue. On the other hand, about 15 stars located on the right side of the dotted line have started the ascent of the RGB and are thus considered as giants.

3. The Lithium main features

Fig. 2 shows the distribution of $A_{\rm Li}$ on the HR diagram and Fig. 3 presents $A_{\rm Li}$ versus log $T_{\rm eff}$ for three ranges of metallicity. The main features presented in Paper I, i.e., the lithium discontinuity around log($T_{\rm eff}$) equal to 3.75, and the dispersion in lithium

Table 1. Derived masses and luminosities for our program stars

HD	$\log(L/L_\odot)$	$M/M_\odot$	HD	$\log(L/L_\odot)$	$M/M_\odot$	HD	$\log(L/L_\odot)$	$M/M_\odot$	HD	$\log(L/L_\odot)$	$M/M_\odot$
400	0.45±0.02	1.0	72954	1.05±0.03	1.6	125451	0.50±0.02	1.3	164507	0.78±0.02	1.4
645	1.36±0.05	1.8	73752	0.55±0.01	1.2	126400	1.22±0.07	1.5	172088	0.73±0.04	1.3
3229	0.99±0.03	1.6	75487	0.90±0.04	1.4	126868	1.28±0.03	2.2	176095	0.91±0.04	1.5
3303	1.45±0.04	1.5	78154	0.60±0.02	1.2	127243	1.74±0.05	2.6	176668	1.37±0.05	2.3
4813	0.21±0.00	1.2	78418	0.58±0.03	1.2	127986	1.08±0.05	1.6	181096	0.73±0.03	1.3
5268	1.71±0.08	1.5	80956	2.09±0.14	3.5	130945	0.92±0.03	1.5	186185	0.81±0.08	1.5
6269	1.65±0.08	2.4	82074	0.98±0.03	1.5	131040	0.68±0.03	1.4	190771	0.05±0.00	1.1
6301	0.64±0.03	1.3	82210	1.21±0.01	1.8	133484	0.78±0.03	1.3	191570	0.55±0.05	1.3
9562	0.60±0.01	1.5	82328	0.88±0.01	1.4	136064	0.66±0.01	1.3	196524	1.38±0.02	1.8
10142	1.69±0.06	2.4	82543	1.72±0.09	2.4	136202	0.70±0.03	1.3	196755	0.90±0.02	1.5
11443	1.11±0.02	1.7	82734	2.05±0.06	3.5	137052	0.93±0.02	1.5	196885	0.40±0.02	1.2
12235	0.56±0.03	1.2	89010	0.55±0.02	1.0	137510	0.68±0.03	1.3	197373	0.50±0.02	1.3
12583	1.70±0.07	2.3	89449	0.62±0.01	1.3	139777	0.02±0.02	1.2	198084	0.96±0.01	1.4
13421	0.92±0.03	1.4	92588	0.59±0.03	1.2	142267	0.01±0.02	1.1	199766	1.33±0.17	1.9
16417	0.45±0.02	1.1	94386	1.34±0.06	1.3	142980	1.56±0.05	2.2	201507	1.22±0.07	1.5
18907	0.65±0.02	1.3	99491	-0.08±0.02	0.8	144070	1.83±0.08	2.6	202582	0.63±0.02	1.2
19826	1.34±0.05	2.2	100219	0.61±0.03	1.3	144284	0.92±0.00	1.5	206901	1.30±0.03	1.6
26913	-0.16±0.02	1.1	102713	1.27±0.04	1.8	144585	0.35±0.02	1.2	207978	0.54±0.02	1.1
26923	0.05±0.02	1.2	104055	2.18±0.14	3.0	150012	1.05±0.05	1.6	208177	1.09±0.05	1.6
27536	1.17±0.04	2.2	104304	-0.00±0.00	1.0	150680	0.89±0.00	1.2	210334	0.80±0.02	1.5
29613	1.49±0.04	2.2	104307	2.05±0.11	2.3	151769	1.17±0.04	1.8	213051	1.43±0.05	1.7
32503	2.23±0.09	3.0	105678	1.08±0.04	1.6	154160	0.51±0.03	1.1	215648	0.65±0.01	1.3
33021	0.41±0.02	1.1	107295	1.96±0.11	3.5	155078	0.92±0.03	1.5	216385	0.70±0.01	1.3
34411	0.28±0.01	1.1	107700	1.86±0.05	2.6	156846	0.71±0.04	1.3	218640	2.50±0.15	4.3
34642	1.19±0.02	1.8	119992	0.36±0.02	1.2	157853	1.83±0.09	2.6	218804	0.4±0.02	1.2
41700	0.22±0.01	1.0	120136	0.46±0.01	1.2	158170	1.31±0.07	1.8	219291	1.44±0.07	2.1
48737	1.01±0.01	1.5	121370	0.97±0.01	1.3	161797	0.43±0.00	1.1	219834	0.55±0.09	1.2
60532	0.97±0.02	1.3	123999	1.10±0.03	1.6	162003	0.75±0.02	1.5	223346	0.78±0.05	1.3
61421	0.81±0.02	1.3	124570	0.74±0.03	1.3	162076	1.53±0.05	2.6			
66011	0.99±0.05	1.5	125184	0.41±0.02	1.1	163989	0.91±0.01	1.5			

abundances for subgiants hotter than this value, clearly appear in both figures.

3.1. Lithium discontinuity

The observational **lithium discontinuity** actually simply reflects the well-known dilution that occurs when the convective envelope starts to deepen after the turnoff and reaches the inner free-lithium layers (Iben 1967a,b). In Fig. 4 we show this behaviour in our models as a function of the effective temperature for different masses. A closer look at the models shows that the beginning of the theoretical lithium dilution is a function of stellar mass, as can be seen in Table 2 where $T_{\rm eff}^{begdil}$ is the effective temperature at the beginning of the lithium dilution for each mass. We also give $T_{\rm eff}^{f10dil}$, which is the effective temperature at which a decrease of the surface lithium abundance by a factor 10 compared to the value on the main sequence is achieved. The dilution is a very fast process, both in terms of age and effective temperature interval. The theoretical beginning of the lithium dilution is in good agreement with the observed abundance drop-off along the subgiant branch, as can be seen in Fig. 5.

For the considered stellar masses, the predicted dilution factor at the end of the dredge-up (see point a on Fig. 4) ranges between 20 and 60 (these values obtained from our models do not significantly differ from the predictions by Iben 1967a,b). This corresponds to the upper envelope of the observations on the right side of the discontinuity, assuming a cosmic lithium abundance $A_{\rm Li}$ of 3.1.

3.2. Lithium dispersion

In the following, we discuss the **lithium dispersion** on both sides of the discontinuity as a function of the stellar mass inferred from the evolutionary tracks at the corresponding metallicity. We select four ranges of mass according to the ones defined in Balachandran (1995) for the cluster and field stars with respect to the so-called lithium dip region (Boesgaard & Tripicco 1986). Each subsample corresponds to peculiar observational behaviour of the $A_{\rm Li}$ on the main sequence (see Fig. 5 where both main sequence and subgiants stars are shown). In the four mass ranges a large dispersion of the lithium abundance appears and is independent of the single or binary status.

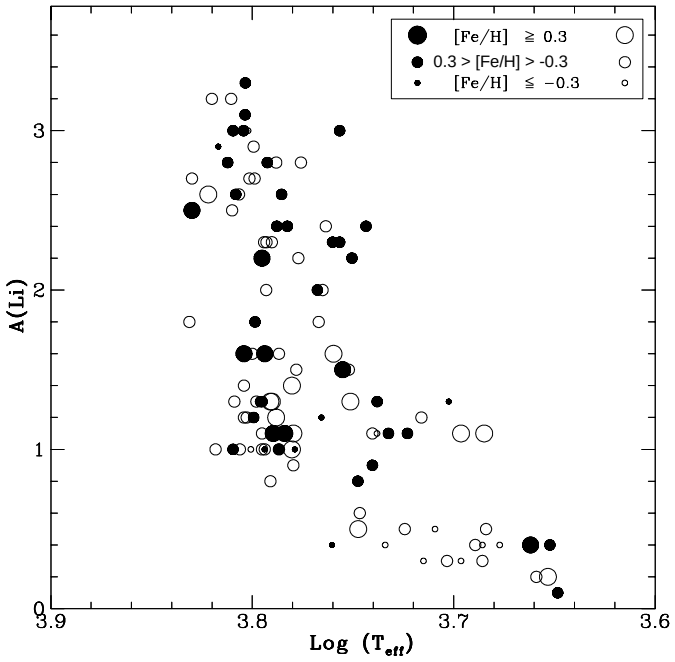

Fig. 3. Lithium abundances as a function of log($T_{\rm eff}$) for all the stars in our sample (Paper I). Open and filled symbols represent single and binary stars respectively. The circle sizes are proportional to the metal content

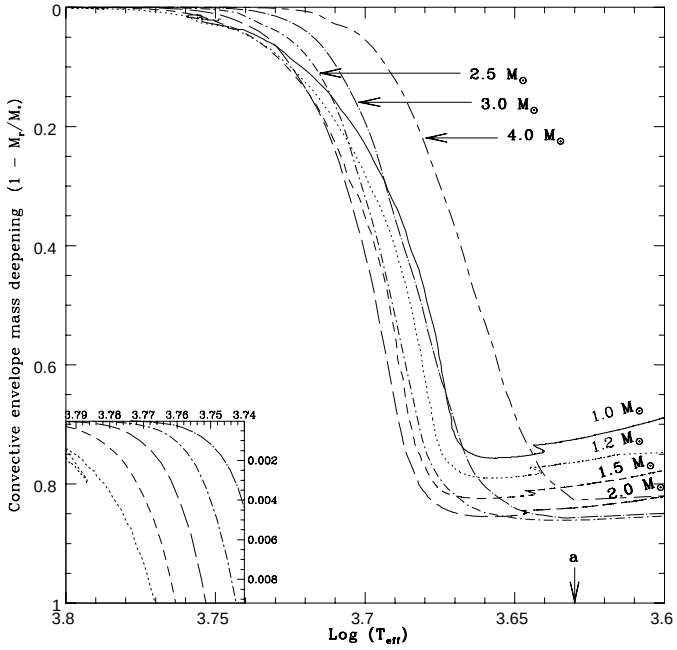

Fig. 4. The deepening (in mass) of the convective envelope is shown as a function of the decreasing effective temperature (first dredge–up) for 1.0 (solid), 1.2 (dot), 1.5 (short dash), 2.0 (long dash), 2.5 (dot - short dash), 3.0 (dot - long dash) and 4.0 $M_\odot$ (short dash - long dash) and [Fe/H] = 0. We present also a zoom of the region $3.80 \geq T_{\rm eff} \geq 3.74$. The point labeled *a* indicates the end of the first dredge-up

Table 2. Relevant characteristics of the models at [Fe/H]=0 shown in Fig. 4. Column 1 gives the stellar masses. Columns 2 and 3 give the effective temperature at the point where the convective envelope just starts deepening and at the onset of the theoretical lithium dilution. The effective temperature at the point where the lithium abundance has decreased by a factor 10 compared to its value at the end of the main sequence is indicated in column 4. Column 5 gives the mass of the convective envelope at the effective temperature of the observed rotational discontinuity

mass ($M_\odot$)	Log $T_{\rm eff}^{dee}$	Log $T_{\rm eff}^{begdil}$	Log $T_{\rm eff}^{f10dil}$	1-$M_{\rm cz}^{Rot}/M_*$
1.0	3.75	3.73	3.68	
1.2	3.79	3.75	3.70	1.70×10^{-3}
1.5	3.79	3.75	3.70	4.31×10^{-4}
2.0	3.77	3.74	3.72	4.22×10^{-5}
3.0	3.75	3.73	3.70	7.00×10^{-7}
4.0	3.74	3.71	3.68	8.00×10^{-7}

(i) Stars with masses < 1.2 $M_\odot$ show different degrees of lithium depletion, which occurs already on the pre-main sequence and on main sequence, as observed in open clusters and field stars (Soderblom et al. 1993; Jones et al. 1999 and references therein). This explains their low lithium content when they reach the subgiant branch (see Fig. 5a).

(ii) Stars with masses between 1.2 and 1.5 $M_\odot$ correspond to the so-called dip region (Boesgaard & Tripicco 1986).

We separate the stars originating from the hot side of the dip region in two mass ranges:

(iii) stars with masses between 1.5 and 2.25 $M_\odot$, and

(iv) above 2.25 $M_\odot$.

We now discuss in more detail the last three cases.

3.2.1. Li-dip stars

Late F- field and open cluster dwarfs with $T_{\rm eff}$ around 6700 K are highly lithium depleted. We find this feature among the dwarfs of our sample which have masses between $\sim$ 1.2 and 1.5 $M_\odot$ (Fig. 5b), in agreement with the observations in the open galactic clusters older than $\sim$ 200 Myr (Balachandran 1995). This lithium depletion persists in our subgiants of the same mass interval, in agreement with the observations in slightly evolved stars of M67 (Pilachowski et al. 1988; Balachandran 1995; Deliyannis et al. 1997). Explanations relying on the nuclear destruction of lithium are thus favoured by these data (see Talon & Charbonnel 1998 and references therein).

3.2.2. Li in stars originating from the hot side of the dip

As can be seen in Fig. 5c,d (see also Fig. 2), a large lithium dispersion exists among our most massive stars, which show lithium depletion by up to two orders of magnitude before the start of the dilution at Log $T_{\rm eff} \simeq 3.75$ (point $T_{\rm eff}^{begdil}$). Very few observational data are available in the literature for stars with masses higher than 1.5 $M_\odot$. In the Hyades, while on the main sequence these objects show lithium abundances close to the galactic value, except for a few deficient Am-stars (Boesgaard 1987; Burkhart & Coupry 1989). However, our observational

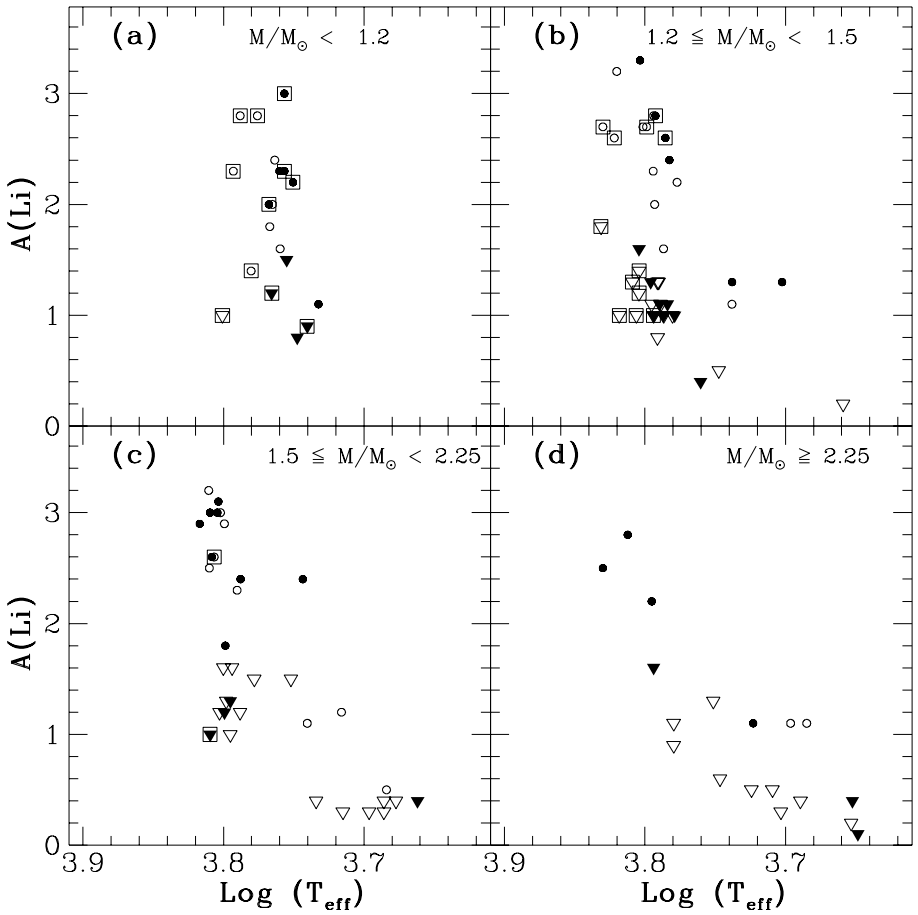

Fig. 5a–d. Lithium abundances as a function of log(T_{eff}) for all our sample stars. Open and filled symbols represent single and binary stars respectively. The circles correspond to lithium detection while inverted triangles are for upper limits in the lithium abundance determination. Squares point out the main sequence stars

result is in agreement with the findings by Balachandran (1990) and Burkhart & Coupry (1991) of a few slightly evolved field stars originating from the hot side of the dip and showing significant lithium depletion. We thus confirm the suggestion by Vauclair (1991, see also Charbonnel & Vauclair 1992) that some extra-lithium depletion occurs inside these stars when they are on the main sequence, even if its signature does not appear at the stellar surface at the age of the Hyades. Among some effects suggested one can quote an unusual mass loss on the main sequence (Boesgaard et al. 1977), and rotational induced mixing (Charbonnel & Vauclair 1992; Charbonnel & Talon 1999).

The behaviour observed in our most massive stars which have not yet reached the beginning of dilution explains the very low lithium content of most of the massive subgiants which cannot be accounted for by dilution alone. The underlying destruction mechanism should also be responsible for the lithium behaviour observed in the Hyades giants (Boesgaard et al. 1977) which have masses higher than 2.25 $M_{\odot}$ and thus correspond to the data we show in Fig. 5d. This process should however preserve the boron abundance, which is in agreement with the standard dilution predictions in the underabundant Li giants of the Hyades, as shown recently by Duncan et al. (1998). Observations of boron in our sample stars have to be done to confirm the similarity between field and cluster evolved stars.

Finally, we note that Non-LTE effects alone can not explain the very low Li abundance derived for several massive stars, as proposed by Duncan et al. (1998). Indeed, Carlsson et al. (1994) have showed that Non-LTE effects can reach up to $\sim +0.3$ dex only for such cool stars. This correction factor is too low to reconcile the derived Li abundances with the standard dilution predictions. Therefore, this confirms that these stars are indeed Li-poor as well as the hotter ones for which only upper limits have been derived (Non-LTE effects are much smaller for such hotter stars).

4. The *Vsini* main features

In Fig. 6 we present the behaviour of rotation in the HR diagram for our sample stars, including the dwarfs and giants. We define several *Vsini* intervals as in Lèbre et al. (1999): Slow rotators correspond to *Vsini* $< 10\ \mathrm{km.s^{-1}}$, moderate rotators to $10\ \mathrm{km.s^{-1}} \leq$ *Vsini* $< 40\ \mathrm{km.s^{-1}}$, and high rotators to *Vsini* $\geq 40\,\mathrm{km.s^{-1}}$. Fig. 6 shows clearly the now well established rotational discontinuity along the subgiant branch near log(T_{eff})=3.79, here indicated by two arrows (Gray & Nagar 1985; De Medeiros & Mayor 1989, 1990). An interesting feature to discuss is the influence of stellar mass on the rotational discontinuity. First of all, one observes that all the subgiant stars with mass lower than about 1.2 $M_{\odot}$ present *Vsini* values lower than 10.0 $\mathrm{km.s^{-1}}$. Observations in young galactic clusters (see Gaigé 1993 and references therein) show that these low-mass stars actually acquire a slow rotation early on the

main sequence, as explained by the magnetic braking scenario for main sequence stars (Kraft 1967; Schrijver & Pols 1993).

Before the rotational discontinuity, the subgiants with mass larger than 1.2 $M_\odot$ present a broad range of *Vsini* values. Because their very thin surface convective envelopes are not an efficient site for magnetic field generation via a dynamo process, these stars are not expected to experience significant angular momentum loss during their main sequence evolution. This result is again in agreement with the data in open clusters.

As can be seen in Table 2 (see also Fig. 4), the effective temperature at which the convective envelope starts to deepen ($T_{\rm eff}^{dee}$) depends slightly on the stellar mass. We also give the depth of the convective envelope at the effective temperature of the rotational discontinuity, $M_{\rm cz}^{Rot}$. For the masses lower than 2.0 $M_\odot$, the observed rotation discontinuity occurs just when the convective envelope starts deepening. We thus see that if the magnetic braking plays a relevant role in the rotational discontinuity, it requires only a very small change in the mass of the convective envelope. Above 2.0 $M_\odot$, our sample is very sparse (due in particular to the very rapid evolution of such stars in the Hertzsprung gap) and we have no data for single stars on the left of the rotation discontinuity exhibited by lower stellar masses. We cannot thus discuss further the impact of the deepening of the convective envelope on the braking in these more massive stars.

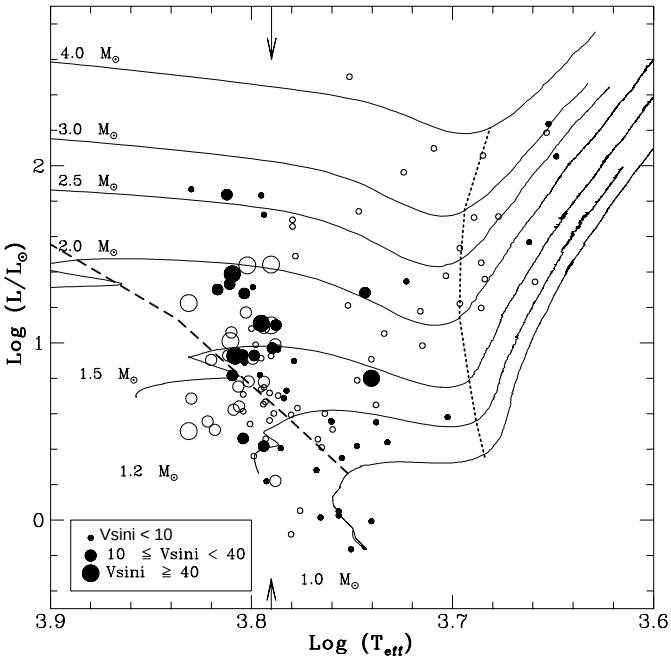

Fig. 6. Rotation for the complete sample. The symbol size is proportional to the rotational velocity measurements (*Vsini*, in $\rm km.s^{-1}$) obtained with the CORAVEL spectrometer by De Medeiros & Mayor (1999).The rotational discontinuity on the subgiant branch (see Paper I) is indicated by the two arrows. Single and binary stars are identified by open and filled circles respectively

5. Conclusions

In this work we have analyzed the Li and rotation observations for 120 subgiant stars from Lèbre et al. (1999). We used the HIPPARCOS trigonometric parallax measurements to locate precisely our objects in the HR diagram and to determine the individual mass and evolutionary status for all stars in the sample.

We have compared observed Li abundances with predictions of Li dilution caused by the deepening of the convective envelope on the subgiant branch. Our models show that the beginning of the theoretical lithium dilution is a function of stellar mass and coincides with the observational features. Stars with masses < 1.2 $M_\odot$ show a large range in abundance before the turnoff, indicating lithium depletion in the previous phases. Stars with masses between 1.2 and 1.5 $M_\odot$ (i.e., in the dip region) show $A_{\rm Li}$ values in agreement with what is found in the open clusters. We note that many stars with masses higher than 1.5 $M_\odot$ show lithium depletion up to two orders of magnitude before the start of the dilution at Log $T_{\rm eff} \simeq 3.75$. The process that depletes Li in these objects while on the main sequence should however preserve the boron abundance, which is in agreement with the standard dilution predictions in the underabundant Li giants of the Hyades, as shown recently by Duncan et al. (1998). Because these specie burn at different depths than lithium, future observations of boron for our sample will provide powerful additional constraints and will confirm the similarity between field and cluster evolved stars.

Our analysis confirms that low mass stars leave the main sequence with a low rotational rate, while more massive stars are slowed only when reaching the subgiant branch. A very slight increase of the depth of the convective envelope seems to be sufficient for the magnetic braking to take place at this phase. Even if the decrease in the behavior of Lithium is nearly the rotational discontinuity, our interpretation of the observations shows that lithium and rotation discontinuities are independent.

Acknowledgements. J.D.N.Jr. acknowledges partial financial support from the CNPq Brazilian Agency. PdL acknowledges partial support grants from the *Société de Secours des Amis des Sciences* and the *Fondation des Treilles*.

References

Alexander D.R., Fergusson J.W., 1994, ApJ 437, 879
Balachandran S., 1990, ApJ 354, 310
Balachandran S., 1995, ApJ 446, 203
Boesgaard A.M., Heacox W.D., Conti P.S., 1977, ApJ 214, 124
Boesgaard A.M., Tripicco M.J., 1986, ApJ 302, L49
Boesgaard A.M., 1987, PASP 99, 1067
Burkhart C., Coupry M.F., 1989, A&A 220, 197
Burkhart C., Coupry M.F., 1991, A&A 249, 205
Buser R., Kurucz R.L., 1992, A&A 264, 557
Carlsson M., Rutten R.J., Bruls J.H.M.J., Shchukina N.G., 1994, A&A 288, 860
Caughlan G.R., Fowler W.A., 1988, Atomic Data Nuc. Data Tables 40, 283
Charbonnel C., Talon S., 1999, in preparation
Charbonnel C., Vauclair S., 1992, A&A 265, 55

De Medeiros J.R., Mayor M., 1989, PASP Conf. Ser. Vol. 9, 6th Cambridge Workshop on: Cool Stars, Stellar Systems and The Sun. p.404
De Medeiros J.R., 1990, Ph.D. Thesis, Geneva Observatory
De Medeiros J.R., do Nascimento J.D. Jr., Mayor M., 1997, A&A 317, 701
De Medeiros J.R., Mayor M., 1991, Angular Momentum Evolution of Young Stars. NATO ASI Series, p. 201
De Medeiros J.R., Mayor M., 1999, A&AS 139, 443
Deliyannis C.P., King J.R., Boesgaard A.M., 1997, In: Kontizas E., et al. (eds.) Wide-Field Spectroscopy. p. 201
Duncan D.K., Peterson, R.C., Thorburn J.A., Pinsonneault M.H., 1998, ApJ 499, 871
ESA, 1997, The Hipparcos and Tycho Catalogues. ESA SP-1200
Gaigé Y., 1993, A&A 269, 267
Graboske H.C., de Witt H.E., Grossman A.S., Cooper M.S., 1973, ApJ 181, 457
Gray D.F., 1981, ApJ 251, 155
Gray D.F., Nagar P., 1985, ApJ 298, 756
Hoffleit D., Jaschek C., 1982, The Bright Star Catalogue. 4th ed., Yale University Observatory, New Haven
Iben I. Jr., 1967a, ApJ 147, 624
Iben I. Jr., 1967b, ApJ 147, 650
Iglesias C.A., Rogers F.J., 1996, ApJ 464, 943
Jones, B.F., Fischer, D., Soderblom D.R., 1999, AJ 117, 330
Kraft R.P., 1967, ApJ 150, 551
Lèbre A., de Laverny P., De Medeiros J.R., Charbonnel C., da Silva L., 1999, A&A 345, 936
Pilachowski C.A., Saha A., Hobbs L.M., 1988, PASP 100, 474
Soderblom D.R., Jones B.F., Balachandran S., et al., 1993, AJ 106, 1059
Schrijver C.J., Pols O.R., 1993, A&A 278, 51
Talon S., Charbonnel C., 1998, A&A 335, 959
Vauclair S., 1991, Proc. of the 14th Symposium of the International Astronomical Union, no. 145, p. 327